ATMOSPHERIC DC CORONA EFFECT IONIZATION AS A POTENTIAL TOOL FOR AEROSOL DEPOSITION: AN EXPERIMENT

Phillip Kauffman
Ionogenics Corp.
San Diego, CA 92130

and

Arquimedes Ruiz-Columbié
Active Influence & Scientific Management
San Angelo, TX 76904

Abstract. High concentrations of ions produced by cosmic rays have an effect on the fair weather electric field which may produce significant and observable changes in local aerosol population properties. Cosmic ray ions may lower nucleation barriers promoting charged nanoparticle growth into the Aitken range and even beyond 100 nm to become cloud condensation nuclei. A twofold assumption was made. On one hand, it was hypothesized that artificially generated direct current corona effect ions would become attached to existing aerosols and these charged aerosols would be far more effective than neutral aerosols in growing via condensation, coagulation and collision which would consequently enhance the deposition rate. On the other hand, the ions may behave as catalyzers of cloud microphysical processes if they reach the cloud bases. This paper evaluates the results obtained in an experiment designed to verify the enounced hypothesis. An ionization station was installed about 8 miles south of downtown Laredo, Texas, in order to measure the impact of unipolar, corona effect ionization on aerosol population and some meteorological phenomena. The station was operated from October, 2005 through August, 2007. Real time airborne spectrometer measurements were obtained and meteorological data were recorded. Data analyzed since the conclusion of the Laredo experiment produced no evidence to support the assumption that ionization had an impact on precipitation, but the hypothesis that ionization does produce gravitational deposition of atmospheric particles was supported by the airborne measurements performed.

1. INTRODUCTION

Man has been fascinated by atmospheric electricity. From the "King of Olympus and Ruler of the Gods", Zeus, God of Sky, Lightning and Thunder, to his Roman counterpart, Jupiter, to the middle age pagan Gods of Lightning, the Nordic God Thor. More recently and crossing the bridge from paganism to science we find perhaps the most talented and accomplished individual of his time inventing the lightning rod after learning how to fly a kite with a heavy metal key attached to it. In the waning days of the nineteenth century, CTR Wilson ran experiments in his cloud chamber and found negative ions to become active at supersaturation rates of 4 and positive ions required a saturation rate of 6 (Wilson, 1897) among many other experiments using his invention.

More recently and more to the point of ionization, in the mid to late 1950's Bernard Vonnegut and C.B. Moore applied ionization technology and conducted experiments that produced unipolar corona effect (CE) ions using a power supply feeding high voltage to a long, thin wire electrically isolated from ground. They used a direct current, high voltage power supply consisting of a step-up transformer and a vacuum tube half wave rectifier to provide pulse energy of either polarity to a thin wire antenna. The wire antenna itself was "T" shaped and the total wire length was about 9 miles. Power was fed in the form of corona discharge pulses 60 times a second. These pulses peaked at about 50KV and the current driven was about 1 x 10^{-3} amp. They were able to detect ions as far as 7 miles away from the ionization station and observed changes in the potential gradient and space charge concentration in ground based as well as airborne measurements (Vonnegut *et al.,* 1962).

2. GALACTIC COSMIC RAYS, AND ALTERNATING AND DIRECT CURRENT IONIZATION

Recent work linking cosmic ray ionization to aerosol behavior led us to believe that corona effect DC ionization might play a substantial role in aerosol deposition. This work is described in the paper submitted by the authors to the American Meteorological Society in January of 2005 (Kauffman and Ruiz-Columbié, 2005).

Corresponding author address: Phillip Kauffman, Ionogenics Corp., 13205 Seagrove Street, San Diego, CA 92130.
E-mail: philkauffman1@gmail.com

Although most ions generated by cosmic rays will be lost because of ion-ion recombination, the few remaining ions will catalyze the nucleation of ultrafine, stable particles (<1-2 nm) by condensation. Most of them will feed larger existing particles (aerosols) thus increasing particle size and catalyzing the process of cloud condensation nuclei (CCN) formation. Some will be scavenged by cloud droplets, contributing to the cleansing effect of depositing small particles (pollutants) on the ground. A fraction of the ultrafine condensation nuclei will again condense and coagulate to form critical embryos (2-5 nm) and a fraction of the former will again coagulate and condense to form cloud condensation nuclei (~100nm). Charged aerosols are more effective in inducing condensation than uncharged ones because polar molecules have an enhanced rate of condensation. Calculations show that this growth rate is greater by a factor of at least 2, and, since a 5 nm particle's coagulation loss rate is 1/20th that of a 1 nm particle, it is an important factor in determining the early survival rate of aerosol (Harrison and Carslaw, 2003).

Aerosols charged by galactic cosmic ray (GCR) ions are far more effective than neutral aerosols in growing via collision. The collision efficiency of a charged aerosol-droplet is increased by thirty-fold for aerosol carrying large (>50) elementary charges (Tinsley and Yu, 2002).

Corona effect is the only method that will produce unipolar ions at a high enough concentration to be useful for aerosol charging (Hinds, 1999). It is probable that unipolar corona effect ions produced by direct current generators will add to and enhance the catalyzing effects that cosmic ray ions produce, including lowering nucleation barriers, increasing the scavenging rate in clouds and, most importantly, stimulating charged particle growth. Since all direct current generated ions will have the same polarity, very few ions will be lost to ion-ion recombination. That means that almost all these small ions are lost only by ion-aerosol combination and ion-droplet attachment in clouds.

Alternating current corona effect ionization produced by high voltage, high power, electrical distribution lines has been linked to polluted aerosol deposition. This type of ionization may improve conductivity in the lower atmosphere by cleaning pollutants which are barriers to the Earth's natural current flow. Alternating current corona effect ionization has been directly correlated to deposition of polluted particles. The model developed by Fews *et al.* (1999) "predicts a two to three-fold increase in deposition of aerosols on spherical surfaces mimicking the human head under high voltage power lines. Experimental measurements using detectors mounted on grounded metal spheres showed an enhanced deposition of both ^{218}Po and ^{214}Po aerosols. The measurements recorded enhanced ^{218}Po and ^{214}Po deposition under 400 kV power lines of 1.96 ±0.15 to 2.86 ±0.32.Enhanced ^{214}Po deposition on 275 kV lines was 1.43 ±0.07".

3. PHYSICAL CONSIDERATIONS ON DC CORONA DISCHARGE

In the vicinity of a corona discharge, the air flow should be considered an electro-hydrodynamic flow in which parameters such as electric and magnetic field intensities, charge distribution, fluid dynamics, and mass and heat transfers play important roles. The Maxwell and Navier-Stokes equations provide the proper background for the solutions, but the problem in general is so complex that it becomes intractable. In the case of a corona generated by a wire under DC high voltage in an open circuit, an electrostatic first approximation for the electric field intensity can be made since electrical currents are negligible. Collisions among charged particles created by the corona (primarily electrons but later other ions) take place thus complicating the process.

In this approximation, the electric potential V is then governed by the Poisson's equation:

$$\nabla \bullet \nabla V = -\frac{\rho_q}{\varepsilon_0} \qquad (1)$$

where ρ_q is the space charge density and ε_0 is the dielectric permittivity of air (≈ 8.85x10^{-12} Fm^{-1}). The electric potential V is associated with the electric field intensity vector by equation 2:

$$\vec{E} = -\nabla V \qquad (2)$$

The electric current density is given then by equation 3:

$$\vec{J} = \mu_E \vec{E} \rho_q + \vec{V} \rho_q - D \nabla \rho_q \qquad (3)$$

where μ_E is the air ion mobility, $\vec{V}$ is the airflow velocity vector and D is the diffusivity coefficient.

In turn, $\vec{V}$ is described by the Navier-Stokes equation (4):

$$\frac{\partial \vec{V}}{\partial t} + \vec{V} \bullet \nabla \vec{V} = -\frac{\nabla p}{\rho_{air}} + \nu \nabla \bullet \nabla \vec{V} - \frac{\rho_q}{\rho_{air}} \nabla \vec{V} \qquad (4)$$

The intrinsic complexity associated with this set of equations lead to numerical modeling. However, here a scaling approach might allow us to estimate the value of the space charge density ρ_q .

From the continuity equation (charge conservation)

$$\nabla \bullet \vec{J} + \frac{\partial \rho_q}{\partial t} = 0 \qquad (5)$$

mathematical manipulations lead to equation 6 (Zhao and Adamiak, 2005):

$$|\nabla \rho_q || \nabla V| \approx \frac{\rho_q^2}{\varepsilon_0} \qquad (6)$$

In cylindrical coordinates this expression becomes

$$\frac{\partial \rho_q}{\partial r} \frac{\partial V}{\partial r} \approx \frac{\rho_q^2}{\varepsilon_0} \qquad (7)$$

Through scale analysis (scaling) one can estimate the magnitude of the terms. For equation 7:

$$\frac{\rho_q}{r} \frac{V}{r} \approx \frac{\rho_q^2}{\varepsilon_0} \qquad (8)$$

Therefore:

$$\rho_q \approx \varepsilon_0 \frac{V}{r^2} \qquad (9)$$

Equation 9 shows an approximated linear relationship between voltage and space charge density. For a voltage of about 70 kV, the space charge density at a distance of 1 m away from the wire results in

$$\begin{aligned} \rho_q &\approx 8.85 \times 10^{-12} \times 7 \times 10^4 Cm^{-3} \\ &\approx 6.2 \times 10^{-8} Cm^{-3} \\ &\approx 3.875 \times 10^{-8} em^{-3} \end{aligned}$$

In the atmospheric boundary layer (ABL) natural ionization is produced by a combination of cosmic rays and radiative gases emanating from the soil. By modeling, Hoppel *et al*., 1986, predicted space charge density of the order of 3×10^9 em^{-3}. In the vicinity of a 70 kV corona discharge the space charge density is about one order of magnitude higher than the value generated by natural resources.

Of course this is an electrostatic approximation and the real world is a hydrodynamic model. Measurements made in the experiment described below detected the influence of high space charge densities at considerable distances from the source of the DC corona generator. The development of a hydrodynamic model for space charge densities using the Maxwell and Navier-Stokes equations, a model supporting the field measurement data, is left for future efforts.

4. CONCEPTUAL MODEL

The conceptual model describes the operation of natural (galactic cosmic ray produced) and anthropogenic direct current CE ionization operating in parallel. Galactic cosmic ray ionization is greater in the upper levels of the atmosphere and only a very small fraction of cosmic rays reach the lower levels of the troposphere. The model is represented in Fig. 1.

In both cases, cosmic ray or corona ions, will quickly (<1s) form ion clusters that have the stability and lifetime to allow them to either attach or grow by condensation and coagulation into stable charged clusters. This will happen in a time-span of a few minutes. In either case the net effect of ionization will be to charge pre-existing aerosols or to form new charged aerosols. Aerosols have lifetimes measured in hours and sometimes days, depending on a wide array of variables.

The illustration in Fig. 2 depicts the conceptual model of microphysical interplay comparing neutral and charged aerosols. Charged molecules

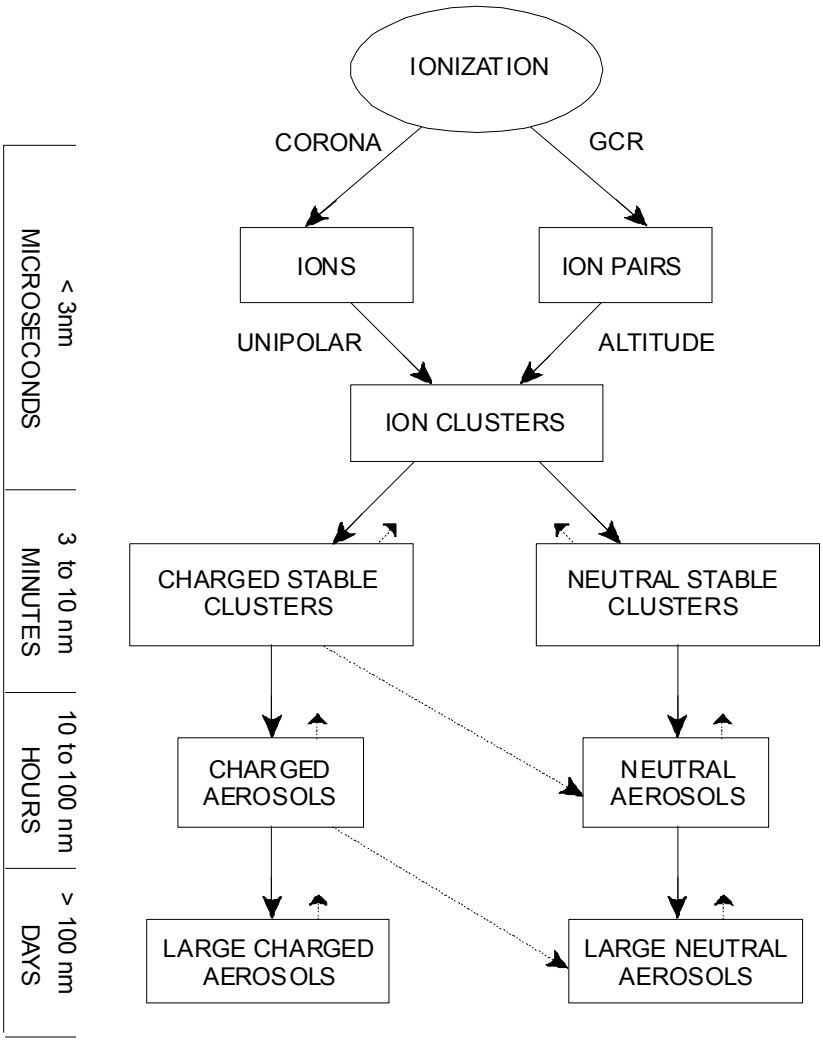

Fig. 1. Block Diagram, Conceptual Model of GCR and DC Corona Ionization

are gray, neutral molecules are white and water molecules are charcoal gray.

For illustration purposes, the model starts with a single aerosol. If there is no charge in the atmosphere, the nucleation process produces new aerosols, however, if ionization is present, the nucleation barriers are lowered, resulting in a larger number of new aerosols. At this point all aerosols are nanoparticles (<10 nm). Within a short period of time neutral aerosols will grow into the Aitken range (10 to 80 nm) and one of the growth mechanisms will be condensation of water vapor. Charged aerosols will grow more aggressively and, if the charge in the aerosols is produced by CE ions, which are more hygroscopic than cosmic ray ions, the condensation growth will be further accelerated. Aerosol growth is also produced by collision and coagulation. Again, in the case of ionized aerosols this growth will be more aggressive. As aerosols become further charged, mirror image charges will be induced in surrounding aerosols to insure collision. The final result is that larger particles are formed under charged atmospheric conditions. Larger particles are made up of orders of magnitude more aerosols than smaller ones. A 100 nm particle CCN is composed of 10^3 nanoparticles, each with a diameter of about 10 nm. The result is that, even though a larger number of nanoparticles are nucleated under charged conditions, the overall particle population is decreased because of two reasons: First, many of the smaller particles have coalesced into larger ones; and second, some of the larger particles are continuously being deposed to ground due mainly to gravitational attraction.

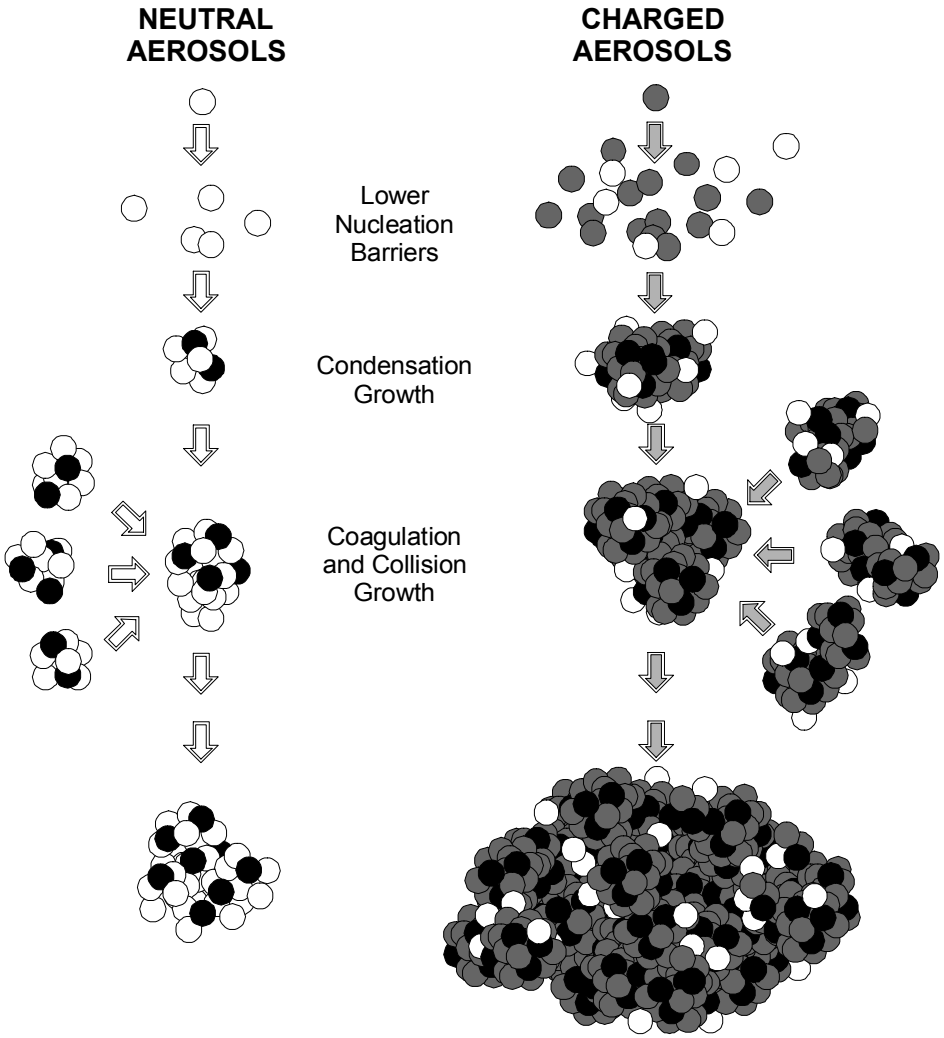

Fig. 2. Illustration of Aerosol Growth, Conceptual Model

5. LAREDO – THE EXPERIMENT

5.1 Preliminary Considerations

The primary objective of this experiment was to measure the impact of the ionization station on precipitation. A secondary goal was to measure any effect attributable to ionization on temperature and the third objective was to observe aerosol size distribution as a tool to provide some insight into ionization plume characteristics.

Particle growth processes induced and aided by corona effect ionization were expected to essentially be the same as for particles ionized by cosmic rays, with the added advantage of unipolarity and thus the avoidance of ion-ion recombination. These growth processes might include condensation, coagulation, coalescence, collision, taking some of the ultrafine (1 – 2 nm) particles to the Aitken range, some of these to the CCN (~100 nm) range, a few of these to the micron level range, possibly resulting in deposition to ground and a few others possibly forming cloud droplets and, ultimately, raindrops.

Precipitation and temperature data along the path of prevailing winds, approximately South to North, would be recorded. There would be two stages for comparing recorded data: One stage would include historical data provided by NOAA, which included precipitation and temperature information from the year 1947 onward. The other stage would be to compare data in a target operational point, Laredo International Airport, with a "control;" or witness point, Cotulla Airport.

The historical precipitation and temperature data provided a framework for predicting rainfall at the target point based on actual rainfall at the witness point and then performing statistical analysis to determine, within a certain level of confidence, whether the actual data was within the limits of natural variation (no ionization effect) or whether it exceeded these limits (due to ionization effect).

Airborne spectrometer data would also be collected to determine particle size distribution in order to determine the range of effectiveness of the ionization plume and to gain insight into the level of ground deposition induced.

5.2 General Description

An ionization station was installed on a farm located off Mangana Hein Road, approximately 8 miles south of downtown Laredo and about 2 miles east of the Mexican border. The official duration of the project was one year, although the experiment was extended another 10 months in order to capture additional data.

The ionization station was comprised of a support structure, a central tower and peripheral towers, which allowed a very long, thin wire antenna to be suspended. The antenna was electrically isolated from the support elements. The antenna was fed by a very high voltage, direct current generator, which was computer controlled to allow for remote operation of the ionization station. The design of the antenna is proprietary and a patent is pending. The antenna design is perhaps the biggest difference between the Vonnegut-Moore antenna (a “T” shaped thin wire with a total wire length of 9 miles) and the antenna used in this experiment, which only had slightly more than 1.5 miles of thin wire, in spite of which the ionization effects were present several tens of miles away. A schematic diagram of the antenna appears in Fig. 3.

Other differences with the Vonnegut-Moore experiment are that their power source provided power pulses at a rate of 60 s^{-1} at 20-50 kV and about 1 mA, whereas the power source used for this experiment provided direct current, continuous power in the range of 70 to 110 kV at 1 to 2 mA. Additionally, the operation for the Laredo experiment was controlled remotely by computer.

Operational and historical precipitation and temperature data was provided by the National Oceanic and Atmospheric Administration (NOAA). Aerosol size distribution data was recorded using a pair of optical spectrometers manufactured by Grimm Technologies (Model number 1109 and 1107). The selection of these spectrometers was based primarily on the real time, optical capabilities of measuring aerosol counts and the adaptability for mounting the instrument on an airplane. The spectrometer’s 31 channel aerosol size selectivity was, at this stage of our work, only of secondary importance. The spectrometers were mounted on the wingtips of a Piper Comanche 260B and the spectrometers were calibrated for the optimum cruise speed of the aircraft and the isokynetic air intake of each spectrometer was adjusted for precisely that speed. See Fig. 4.

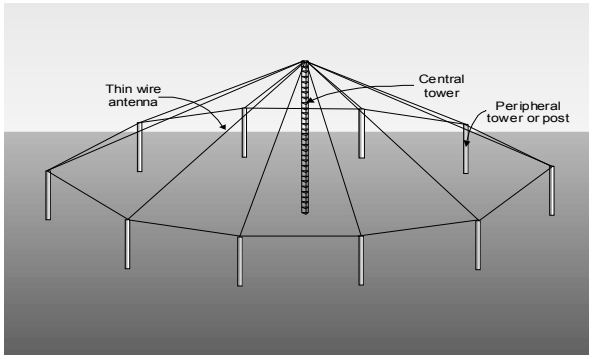

Fig. 3. Antenna Schematic

Since the main focus of the experiment was to evaluate the precipitation enhancement capability of the ionization station, all flight data was recorded between 2,000 and 3,500 feet, at the approximate base of rainfall producing stratus, stratocumulus and nimbostratus clouds.

Fig. 4. Piper Comanche 260B, Equipped with Two Wingtip Mounted Spectrometers

The map in Fig. 5 shows the approximate location of the ionization station, the operational point (LRD – Laredo International Airport), the witness point (Cotulla), the prevailing wind direction during the summer and the preliminary expectation of the coverage of the ionization plume.

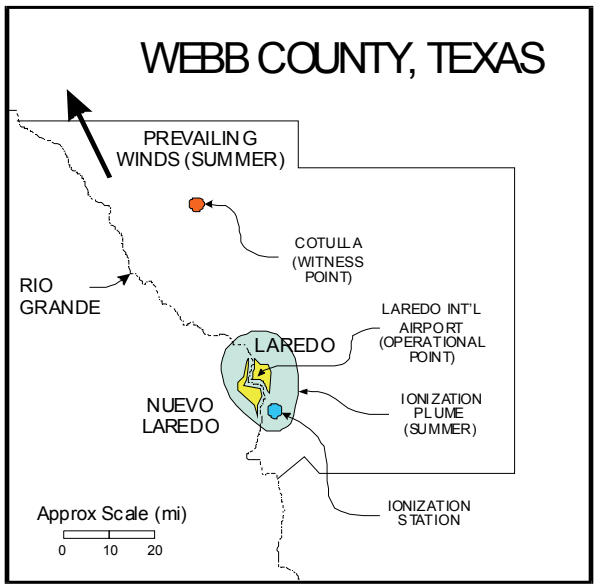

Fig. 5. Ionization Station Map

5.3 Data: Precipitation

Precipitation data were recorded during the experiment for the operational point, Laredo, and the control, or witness point, Cotulla. Rain gage values of precipitation, provided by NOAA, for the Hydroyear 1947-1997 (defined as the 12 months between Oct 1 and Sep 30 of the next year) at Cotulla and Laredo were used to obtain an evaluation of the apparent impact of the ionization station. The analysis also included a detailed description using some percentiles of the precipitation distributions in both areas. This methodology allowed us to classify every month during the aforementioned period as very dry, dry, normal, wet and very wet (Ruiz-Columbié *et al.*, 2006).

The average precipitation in Laredo for the hydroyears 1947 to 1997 is 19.96. The historical precipitation percentiles for Laredo are provided in Tables 1a & 1b.

Table 1a. *Percentile Boundaries, Laredo*

13.86 in (20th percentile)
16.43 in (40th percentile)
21.15 in (60th percentile)
24.89 in (80th percentile)

Table 1b. *Historical Precipitation Levels – Laredo*

Very Dry	(precip < 13.86 in)
Dry	(13.87 < precip < 16.43 in.)
Normal	(16.44 < precip < 20.04 in.)
Wet	(20.05 < precip < 21.15 in.)Very
Wet	(21.16 < precip < 24.89 in.)

Precipitation for Laredo during the experiment's hydroyear (defined for this project as Oct 1, 2005 through Sep 30, 2006) was 14.88, which categorizes it as "Dry".

The average precipitation in Cotulla for the hydroyears 1947 to 1997 is 20.68. The historical precipitation percentiles for Cotulla are:

Table 2a. *Percentile Boundaries, Cotulla*

16.27 in (20th Percentile)
18.84 in (40th Percentile)
20.69 in (60th Percentile)
24.38 in (80th Percentile)

Table 2b. *Historical Precipitation Levels – Cotulla*

Very Dry	(precip < 16.27 in)
Dry	(16.28 < precip > 18.84 in.)
Normal	(18.85 < precip > 20.68 in.)
Wet	(20.69 < precip > 24.38 in.)
Very Wet	(24.39 < precip > 28.28 in.)

Precipitation for Cotulla during the experiment for the hydroyear was 24.53, which qualifies the year as "Wet". The regression analysis offered the following results: The linear correlation coefficient r = 0.71 indicates good correlation. Based on Cotulla's actual precipitation of 24.53 inches for the hydroyear of the experiment, the expected precipitation level for Laredo was 21.55. The equation used is:

Laredo Expected Prec. = 0.70 x Cotulla Actual Prec. + 4.38 = 0.70 x 24.53 + 4.38 = 21.55 (1)

The actual precipitation was 14.88, which is 6.67 inches below the expected level. The Working Hotelling amplitude (at the 95% confidence level) is 1.52 (Working and Hotelling, 1929) which means that the precipitation decrease is significant.

The above analysis clearly shows that precipitation in Laredo for the hydroyear Oct 05 through Sep 06 was not enhanced. It was, in fact, significantly below the historically predicted level. The annual report to the TDLR also states that the choice of Cotulla as a witness point was a mistake and that it was strongly suspected that Cotulla was well within the influence zone of the ionization station.

5.4 Data: Aerosol Size Distribution - General

The basic flight plan used was designed to attempt to capture data both in the operational as well as the control (witness) areas by flying over the longest axis of the ionization plume. It is shown in the map in Fig. 6.

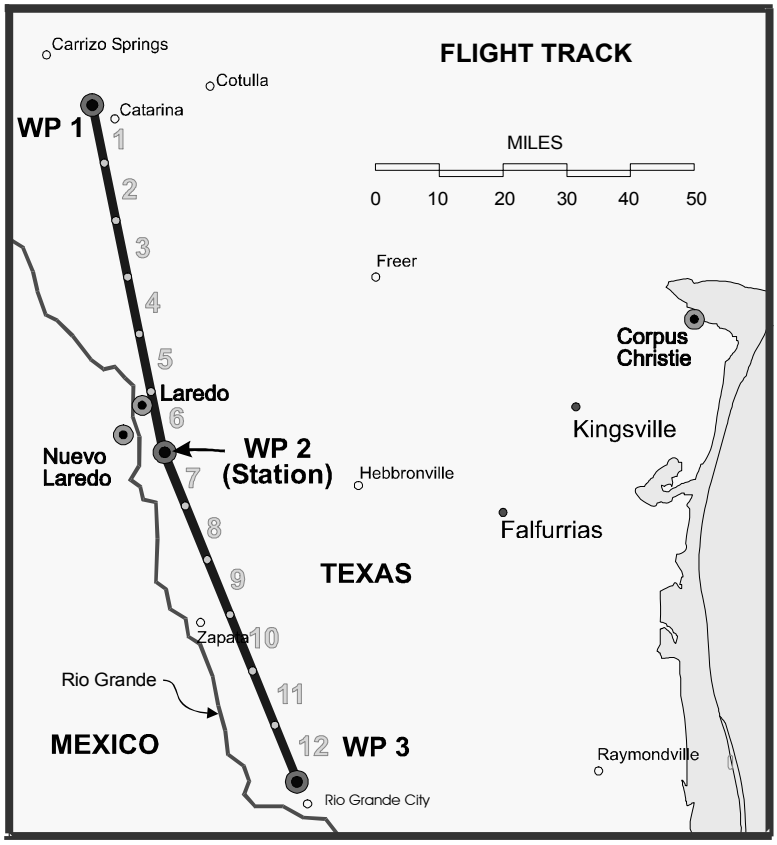

Fig. 6. Measurement Flight Plan

The aircraft starts its measurement run at Waypoint 1, West of Cotulla, proceeds to Waypoint 2, which is the location of the ionization station, then on to Waypoint 3, close to Rio Grande City. Airspeed and altitude are maintained by the airplane's autopilot in order to stay within limits required by the spectrometer's isokynetic air intake. The total length of the flight path is about 120 miles.

Each spectrometer is designed to measure atmospheric particles in 31 channels ranging from 250 nm to 32 microns. Readings are taken every 6 seconds and the data are presented as number of aerosols per liter. In order to simplify viewing and analyzing the data, the particle sizes were reduced from 32 channels to 4: Small (0.0 to 0.280 μm), Medium (0.281 to 0.350μm), Large (0.351 to 0.800 μm) and Giant (0.801 to 32.000 μm). This allows viewing 4 graphs instead of 31. Further simplification resulted from dividing the flight path into 12 flight zones, each one about 10 miles long, and the recorded data were averaged for each flight path, thus reducing the number of data points from around 700 to 12.

All measurement flights were analyzed, verifying a number of parameters, among them, flight recorder data including coordinates, altitude and groundspeed, cloud formations observed by the pilot during flight. Background conditions were also analyzed, including 24 hour backward wind trajectories at waypoints 1, 2 and 3 NOAA HYSPLIT Model (Draxler and Rolph, 2003), atmospheric background, including NAAPS (Navy Aerosol Analysis and Prediction System) images for optical depth and sulfate, dust and smoke concentrations. Also, any unusual conditions encountered during flight were reported by the pilot to rule out anomalies such as vehicular or cattle traffic which might impact the measurements. An example of typical HYSPLIT Model backward wind trajectories (BWT) appears in Fig. 7, which shows the BWT for Waypoints 1, 2 and 3.

An example of the NAAPS background is provided in Fig. 8.

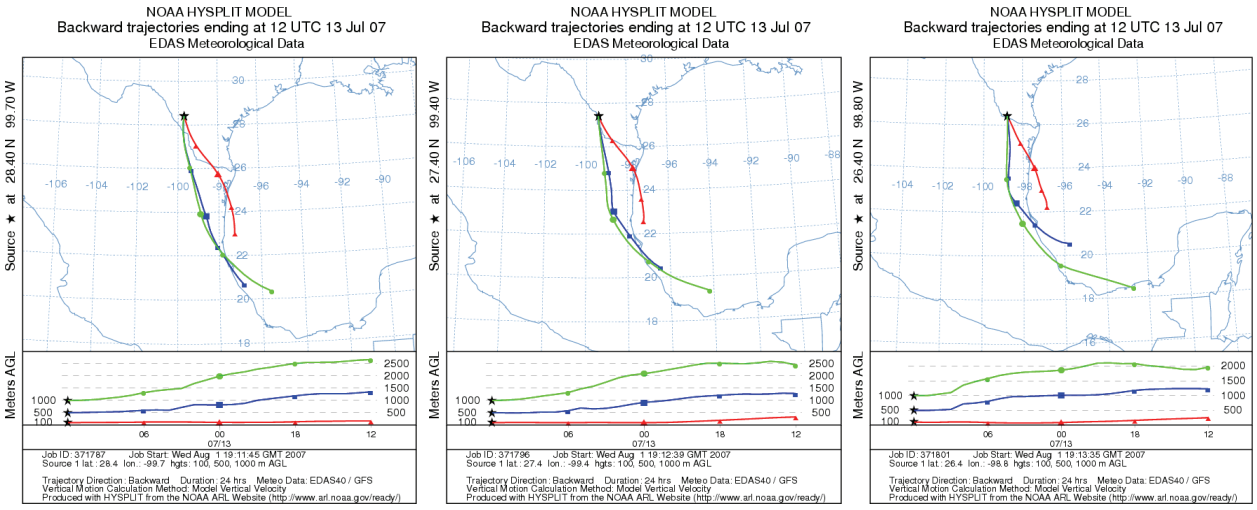

Fig. 7. HYSPLIT Model Backward Wind Trajectories, 07/13/2007, WP 1, WP 2 and WP 3

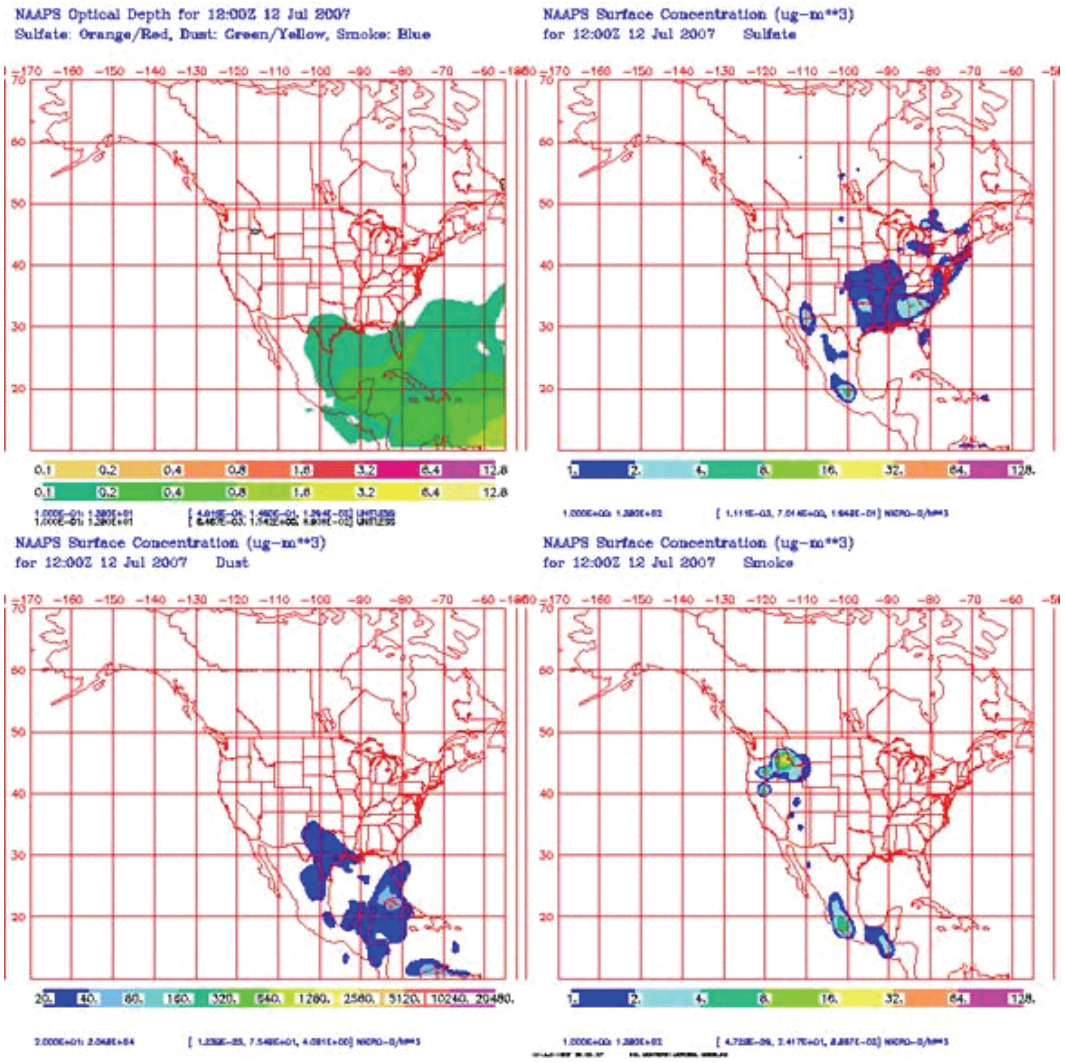

Fig. 8. NAAPS Background Information, April 14, 2006, 12:00 Z

There were a total of three sets of measurement flights performed: One set, called "Zero Operation" when the ionization station is turned off, another set called "Positive Operation" with the station operating on positive polarity, and, a third set called "Negative Operation" where the station was operating on negative polarity.

Data was further simplified in order to allow graphic analysis. Because of the very large variability in atmospheric conditions from day to day and because it was necessary to compare flights performed in different dates, all data was normalized so that the maximum particle count reading for each flight was forced to a value of 1.00 (or 100%). Further, the four particle size ranges was reduced to one in order to analyze the relative total number of atmospheric particles along the measurement flight path in a simple and straightforward fashion.

In order to switch from operational or non-operational state a period of transition to achieve steady state conditions was required. It was estimated that to go from an operational state (either positive or negative) to a non-operational state it would take about 20 hours at a constant wind speed of 3m x s^{-1} to travel 200 km (about 120 miles) provided there was no change in wind direction (Time = (100 x 1000) / 3 = 66,000 seconds = 66,000 / 3,600 = 18.3 hours. If wind speed and direction change it would take longer to "sweep" the ionized air away. Similarly, for non ionized air to charge the ionized aerosols must be transported by the wind, but an additional time period is required for aerosols to grow to a point where aerosol deposition reaches a steady state value. For purposes of this experiment, it was deemed that a period of transition of about 96 hours would be enough to achieve substantially steady state conditions when switching from one operational state to another.

The historical (1947 to 1998) prevailing wind direction in Laredo for the months of February through September is SSE, approximately 155°. Due to some difficulties pointed out by our pilot, the flight plan was designed slightly off the prevailing wind vector at approximately 160° for flight zones 12 through 7 and 170° for flight zones 6 through 1.

All flights were performed during the months of February through August. All flights were scheduled during the morning hours to avoid, where possible, measurements after convection had started in earnest. The overall predominant wind direction for all flight days was from the ESE (approximately 125°), which means that the flights did not cut the ionization plume along it's predicted major axis, although the directional difference did allow the flights to measure along much of the length of the plume.

5.5 Data: Aerosol Size Distribution – Non Operational

Because maritime atmosphere is less polluted than continental atmosphere, the expectation was that the total number of particles in suspension would increase as the aircraft went further inland and would decrease as the aircraft approached the coast.

As can be seen from the previous Alpha Flight Plan map in Fig. 6, the aircraft is closer to the coast at WP 3 (Flight Zone 12) than it is at WP1 (Flight Zone 1). In fact, WP 3 is about 60 miles closer to the Gulf coast than WP 1. Therefore, for the case where the ionization station is turned off (non-operational), the expected total number of particles at Flight Zone 12 should be lower than at Flight Zone 1. In order to test this hypothesis, normalized data was used to compare flights performed on different days. The goal was to see how the total number of aerosols increase or decrease along the flight path.

The average normalized data of all six non-operational flights is depicted in the chart in Fig. 9.

Fig. 9 shows the average aerosol counts (pink line) average plus one standard deviation (brown line) and average minus one standard deviation (blue line). It is obvious that aerosol counts vary greatly for natural, non operational atmospheric conditions and so the standard deviations are quite large. Fig 9 also shows a linear trendline, its equation and a good correlation of 0.82. The trendline clearly supports the hypothesis that aerosol counts increase as the atmosphere becomes more continental and less maritime. The rate of increase in aerosol counts is about 3.4% for every ten miles traveled along the flight path described in Fig. 6.

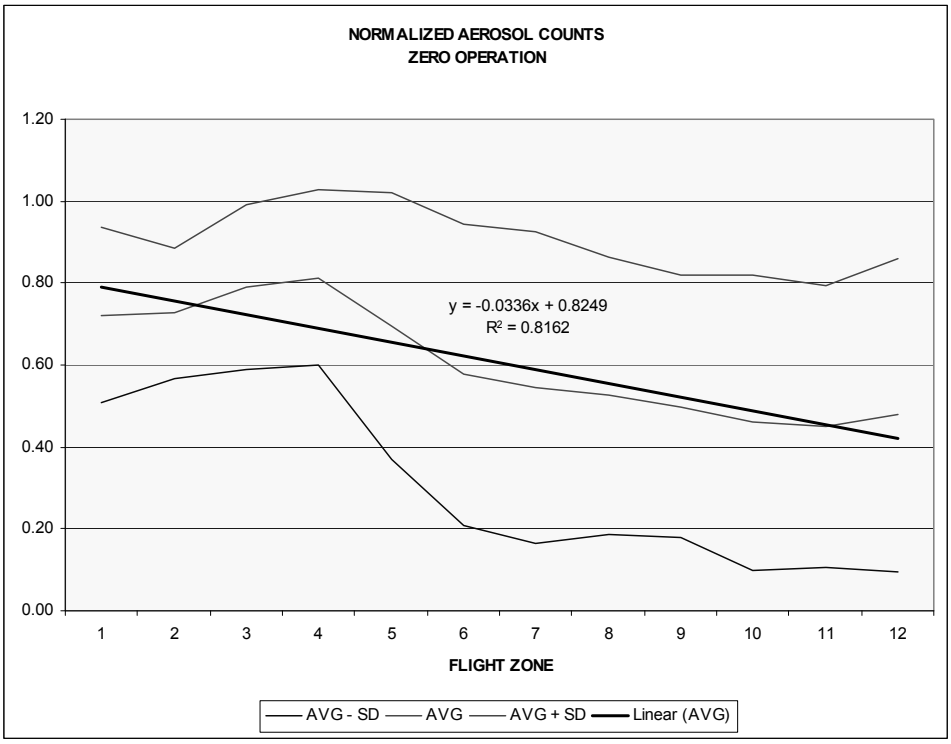

Fig. 9. Average Normalized Flight Measurement Data – Non Operational

5.6 Data: Aerosol Size Distribution – Operational Negative

When operating the station it was logical to assume that in either mode of operation, positive or negative, the number of aerosols measured in Flight Zone 1 would be less than the ones measured in Flight Zone 1 for non-operational conditions. This is because ionized aerosols grow more aggressively than electrically neutral ones. Part of this growth is by coagulation, which should substantially lower the number of smaller aerosols. Larger aerosols would also be more likely to depose to ground over a period of time due to gravity. The normalized data recorded for the four flights for negative operation are shown in Fig. 10. It is clear that there is a significant reduction in the number of aerosols measured in Flight Zone 1. Furthermore, the slope of the linear trendline went from negative under non-operational conditions to positive under negative operation. Additionally, it appears that standard deviations are smaller and perhaps growing smaller even as the flight zone numbers decrease, which are the areas where ionization is producing larger effects.

5.7 Data: Aerosol Size Distribution – Operational Positive

When analyzing positive operation, one would expect results to be similar to negative operation, since what is most important in either mode of operation is that all CE ions are unipolar. The normalized data for the eight flight segments measuring aerosol counts during positive operation are shown in Fig. 11.

As shown in Fig 11, the decrease in the number of measured aerosols from Flight Zone 12 to Flight Zone 1 is larger than for negative operation. In both negative and positive polarity there is deposition of aerosols caused by the aggressive growth of charged aerosols which increases gravitational attraction and, consequently, their downward vertical velocity. However, during negative operation, negatively charged aerosols are repelled by the negatively charged ground, whereas under positive operation, positively charged aerosols are attracted to ground. Thus, in the case of negative operation deposition is the result of gravity less electrical repulsion, whereas in positive operation, deposition is the result of gravity plus electrical attraction.

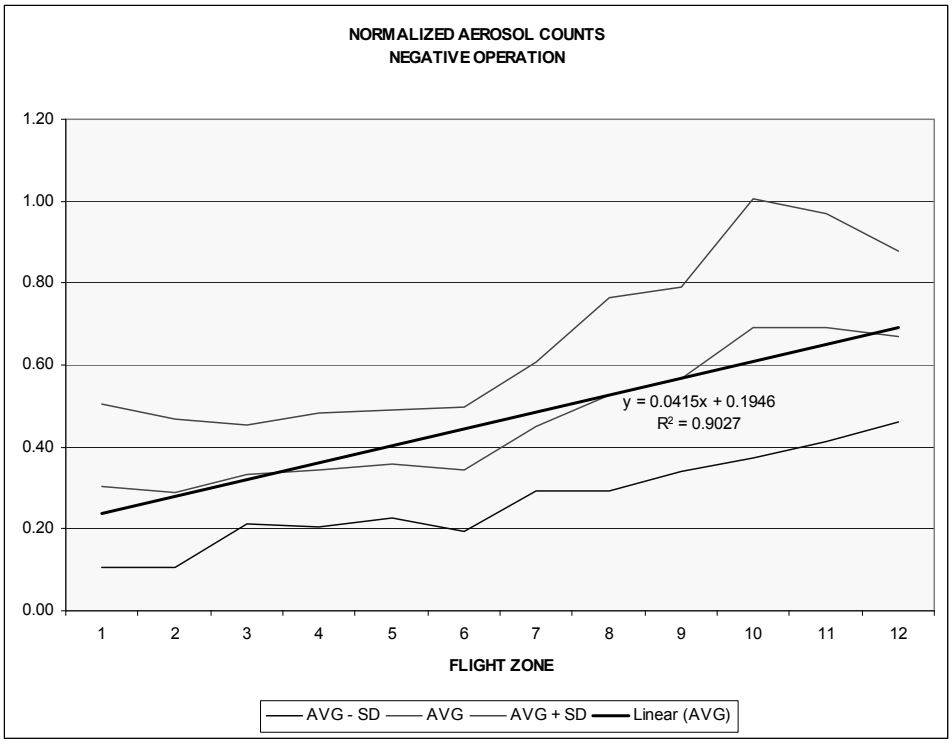

Fig. 10. Average Normalized Flight Measurement Data – Operational, Negative

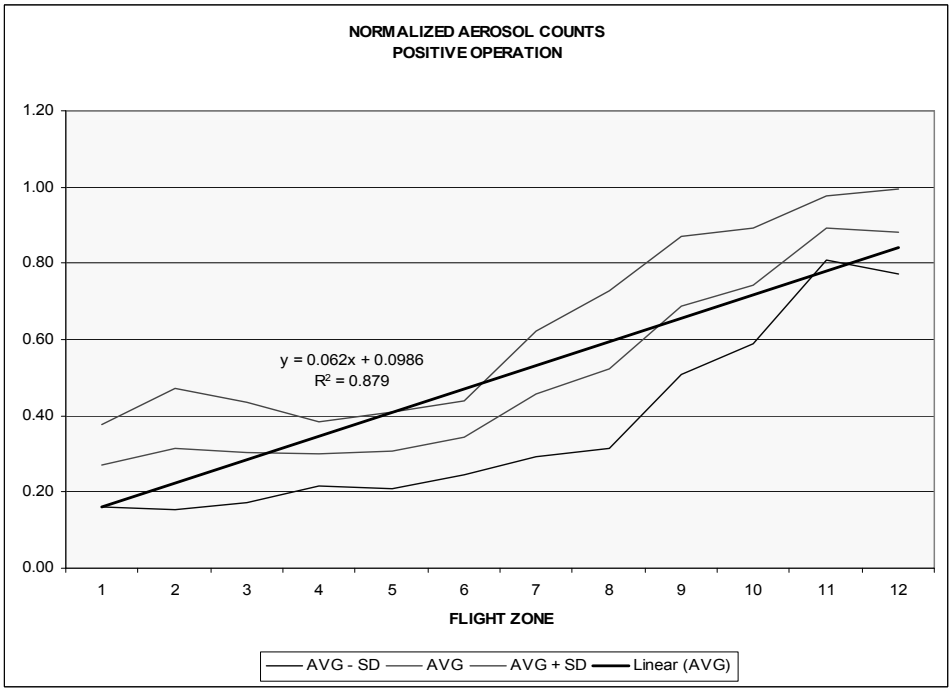

Fig. 11. Average Normalized Flight Measurement Data – Operational, Positive

5.8 Data: Aerosol Size Distribution – Flights Extended to the Gulf Coast

Additional flights were also performed extending the flight to the Gulf Coast after completing the normal Flight Zone 1 thru 12 track. This added flight zones 13 to 19 heading straight East from flight zone 12 and flight zone 20 heading North from flight zone 19. Two of the flights were under non operational conditions and one was operational. The flight track is depicted in Fig 12.

Flight data for segments 1 through 12 of these flights have been included in the previously described analysis, but looking at all 20 flight zones may prove interesting.

The non operational flight data for flights with an extension to the Gulf Coast are charted in Fig 13.

It would appear that the number of aerosols does, in fact, increase as the air becomes less maritime and more continental. There is an increase of about 70% in the number of aerosols measured in Flight Zone 1 from the number measured in Flight Zone 12.

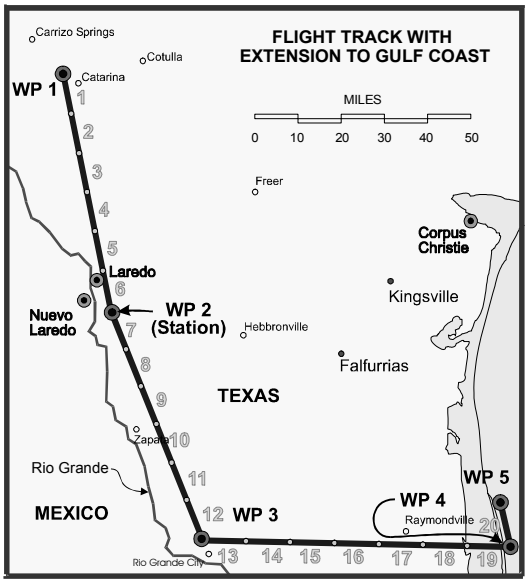

Fig. 12. Flight Track with Gulf Coast Extension

Another flight with a Gulf Coast extension was performed when the station was operational with positive voltage. The results are shown on Fig 14.

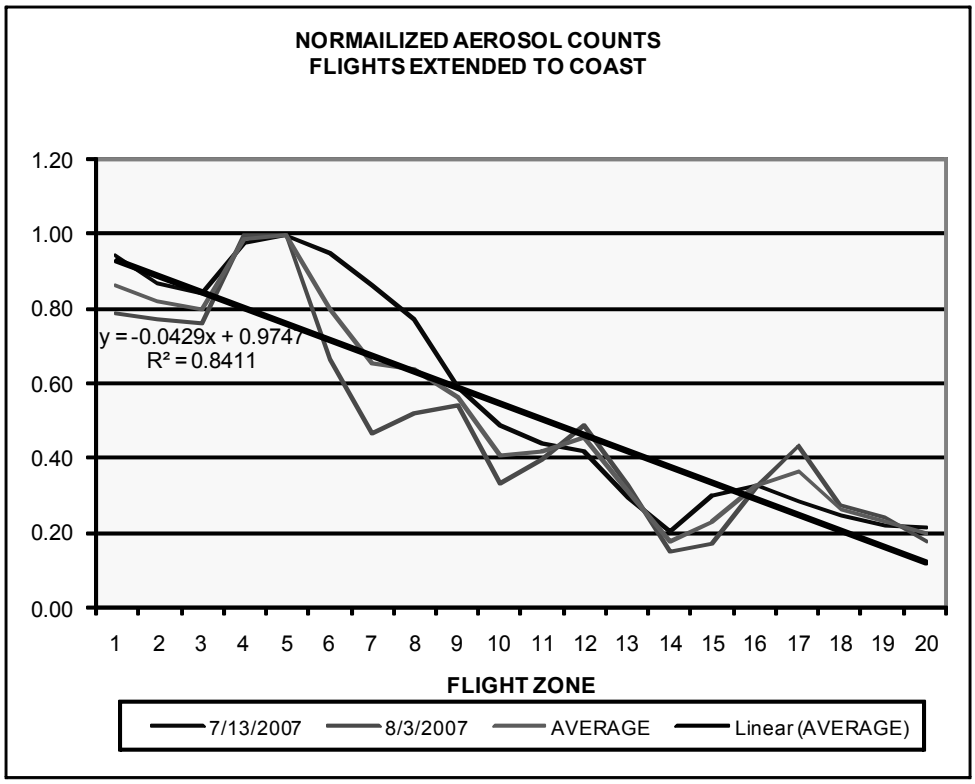

Fig. 13. Normalized Aerosol Counts – Flights extended to the Coast- Zero Voltage

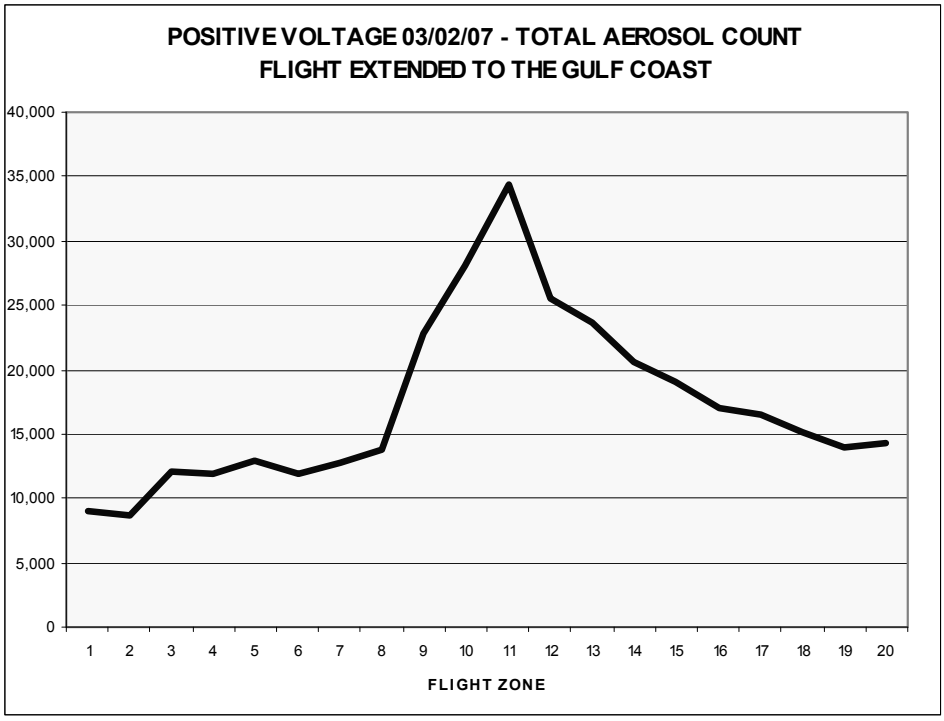

Fig. 14. Flight extended to Coast – Positive Voltage

The graphic indicates that there are two distinct patterns: The first one, going from Flight Zone 1 to Flight Zone 11, shows that aerosol counts are increasing. This is due to the effect of ionization. The second pattern, going from Flight Zone 12 to Flight Zone 20, shows decreasing aerosol counts, substantiating the hypothesis that maritime air is cleaner (less aerosols) than continental air.

5.9 Data: Aerosol Size Distribution – Operational vs. Non Operational

In order to visualize the effect of the ionization station on aerosol counts, a final data manipulation was performed. The normalized data for all three operational states at Waypoint 3, the start of Flight Zone 12, was forced to equal 1.0 and then all the rest of the normalized data for each Flight Zone was plotted, based on the common Waypoint 3 starting point. Waypoint 3 is clearly well outside the area of influence of the ionization station so that the readings at that waypoint would be the same, whether the station was operating or not.

Another simplification was made in that operational data for positive and negative operation were combined so that a comparison of "Operational vs. Non Operational" conditions can be made in a straightforward manner. The result is shown in Fig. 15.

It seems clear that ionization does not truly start to influence aerosol populations beyond zone 10, so that the area of ionization influence appears to be from Flight Zone 1 through Flight Zone 9, a distance of approximately 90 miles.

It is interesting to observe that the "bandwidth" between plus and minus one standard deviation for non operational conditions is much wider than the corresponding operational bandwidth. Although the bandwidth is tighter the closer we come to Flight Zone 1, at Flight Zone 12, where there is, presumably, no ionization effect, the bandwidth is still tighter for operational conditions than for non operational conditions.

The efficiency of ionization in aerosol reduction can be calculated by obtaining the ratio of Operational and Non-Operational normalized aerosol counts for each flight zone and subtracting 1. The results can be read as the efficiency of the Operational Mode in increasing (positive efficiency number) or decreasing (negative efficiency number) aerosol counts in the corresponding Flight Zone. The results are reflected in Table 2.

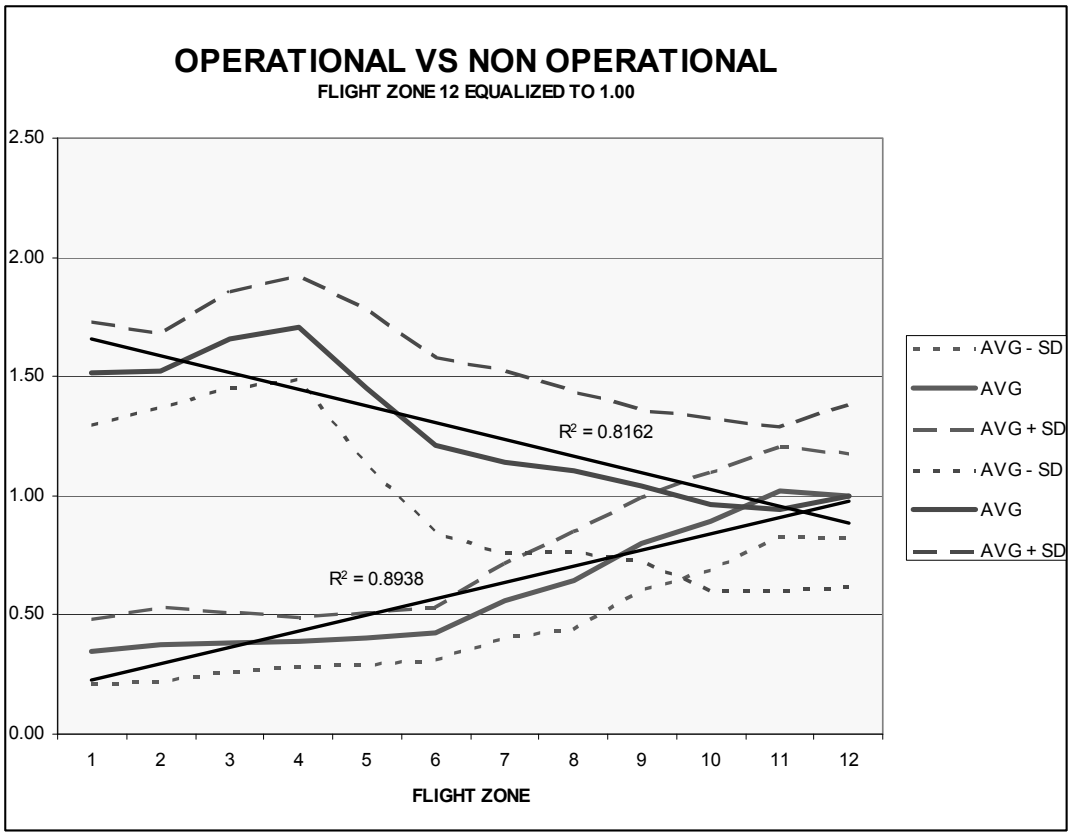

Fig 15. Average Normalized Flight Measurement Data Comparison of Non Operational and Operational Modes

Table 2. Operational Ionization Efficiency

ZONE	OPER AVG	NON OP AVG	RATIO OP TO NON OP	EFFIC'Y PCT
1	0.35	1.51	0.23	-77%
2	0.38	1.52	0.25	-75%
3	0.39	1.65	0.23	-77%
4	0.39	1.70	0.23	-77%
5	0.40	1.45	0.28	-72%
6	0.42	1.21	0.35	-65%
7	0.56	1.14	0.49	-51%
8	0.65	1.10	0.59	-41%
9	0.80	1.04	0.76	-24%
10	0.89	0.96	0.93	-7%
11	1.02	0.94	1.08	8%
12	1.00	1.00	1.00	0%

An approach can be made toward the interpretation of Fig. 15 by assuming a normal distribution and using a Fermi question approach to examine the probabilities of occurrence of the events recorded (Morrison, 1963). To do this we need to determine how far away the Non Operational mean is from the Operational mean, in units of standard deviation. The equation that is used for this is:

$$\text{Op Mean} = \text{Non Op Mean} - Z \times \text{Non Op Std Dev} \quad (1)$$

From eq (1), multiplying both sides by -1:

Z = Distance between Op and Non Op Means = (Non Op Mean – Op Mean) / Non Op Std Dev

The results are displayed in Table 3.

Table 3 shows that Flight Zones 10, 11 and 12 are naturally occurring events, while zones 1 through 8 are probably not. It is also evident that zones 1 through 5 are more than 3 standard deviations apart. Flight Zone 9 is the transition point.

6. CONCLUSION

A number of direct and indirect references have been made to recent publications which point out the ever more widely accepted postulate that ionization contributes to more aggressive aerosol growth. Growth that is accomplished not by one or two but by all growth mechanisms observed to date, including condensation, coagulation, coalescence, scavenging and collision/aggregation. The data charted in Fig. 10. provide an additional pebble on the road to understanding aerosol properties by showing that it is probable that aerosol growth leads to a reduction of aerosol counts because smaller aerosols are “feeding” larger, charged, aggressively growing aerosols and these larger aerosols will likely enhance gravitational deposition, which is recorded in proxy data as an overall reduction in the number of aerosols in the atmosphere surrounding an ionization station, preferentially upwind of the station.

REFERENCES

Draxler, R.R. and G. D. Rolph, 2003: HYSPLIT – Hybrid Single Particle Integrated Trajectory Model; NOAA Air Resources Laboratory, Silver Spring, MD, http://www.arl.noaa.gov/HYSPLIT.php

Fews, A.P., D.L. Henshaw, P.A. Keitch, J.J. Close, and R.J. Wilding, 1999: Increased exposure to pollutant aerosols under high voltage power lines. *Int. J. Radiat. Biol*., **75**, 1505-1521.

Table 3. Probability of Natural Occurrence of Figure 15 Results

FLIGHT ZONE	NON OP STD DEV	NON OP MEAN	OP'L MEAN	Z NUM OF STD DEVS	PROB'Y OF OCCUR
1	0.21	1.51	0.34	5.57	0.00
2	0.15	1.52	0.37	7.67	0.00
3	0.20	1.65	0.38	6.35	0.00
4	0.21	1.70	0.38	6.29	0.00
5	0.32	1.45	0.40	3.28	0.00
6	0.36	1.20	0.42	2.17	0.02
7	0.38	1.14	0.56	1.53	0.06
8	0.33	1.10	0.64	1.39	0.09
9	0.31	1.04	0.79	0.81	0.22
10	0.36	0.96	0.89	0.19	0.42
11	0.34	0.94	1.01	-0.21	0.59
12	0.38	1.00	1.00	0.00	0.50

Harrison, R. G. and K. S. Carslaw, 2003: Ion-Aerosol-Cloud processes in the lower atmosphere. *Rev. of Geophys.*, **41**, 3 / 1012-1038.

Hinds, W.C., 1999: *Aerosol Technology: Properties, Behavior and Measurements*, Second Edition, John Wiley and Sons, Inc., pp 331.

Hoppel, W.A., G.M. Frick, and R.E. Larson, 1986: Effect of nonprecipitating clouds on the aerosol size distribution in the marine boundary layer. *Geophys. Res. Lett.*, **13**, 125-128.

Kauffman, P. and A. Ruiz-Columbié, 2005: Artificial atmospheric ionization: A potential window for weather modification. *16th Conference on Planned and Inadvertent Weather Modification,* Am. Met. Soc., http://ams.confex.com/ams/pdfpapers/88063.pd

Morrison, P., 1963: Letters to the Editor, *Am. J. Phys.*, **31**, 626-627.

Ruiz Columbié, A., L. Grave de Peralta, and G. Farazoulis, 2006: Coping with precipitation variability. *Journal of Weather Modification*, **38**, 97- 104.

Tinsley, B. A. and F. Yu, 2002: Atmospheric ionization and clouds as links between solar activity and climate, http://www.utdallas.edu/dept/physics/Faculty/tinsley/Atmos_060302.pdf

Vonnegut, B. *et al*., 1962: Artificial modification of atmospheric space charge. *J. of Geophys. Res.,* **67**, 1073.

Wilson, C.R.T., 1897: Condensation of Water Vapour in the Presence of Dust-free Air and Other Gases, *Phil. Trans*. **A, 189**, 205.

Working, H. and H. Hotelling, 1929: Applications of the theory of error to the interpretation of trends. *Journal of the American Statistical Association*, **24**, 73-85.

Zhao, L. and K. Adamiak, 2005: Effects of EHD and external air flows on electric corona discharges in pin-plate configuration. Conference Record of the IEEE-IAS 2005 Fortieth Annual Meeting, Hong Kong, Volume 4, pp 2584-2589.